

APPLIED SCIENCES AND ENGINEERING

Self-targeting, zwitterionic micellar dispersants enhance antibiotic killing of infectious biofilms—An intravital imaging study in mice

Shuang Tian^{1,2}, Linzhu Su^{1,2}, Yong Liu^{1,2*}, Jingjing Cao¹, Guang Yang^{1,2}, Yijin Ren³, Fan Huang⁴, Jianfeng Liu^{4†}, Yingli An¹, Henny C. van der Mei^{2†}, Henk J. Busscher^{2†}, Linqi Shi^{1†}

Extracellular polymeric substances (EPS) hold infectious biofilms together and limit antimicrobial penetration and clinical infection control. Here, we present zwitterionic micelles as a previously unexplored, synthetic self-targeting dispersant. First, a pH-responsive poly(ϵ -caprolactone)-*block*-poly(quaternary-amino-ester) was synthesized and self-assembled with poly(ethylene glycol)-*block*-poly(ϵ -caprolactone) to form zwitterionic, mixed-shell polymeric micelles (ZW-MSPMs). In the acidic environment of staphylococcal biofilms, ZW-MSPMs became positively charged because of conversion of the zwitterionic poly(quaternary-amino-ester) to a cationic lactone ring. This allowed ZW-MSPMs to self-target, penetrate, and accumulate in staphylococcal biofilms *in vitro*. *In vivo* biofilm targeting by ZW-MSPMs was confirmed for staphylococcal biofilms grown underneath an implanted abdominal imaging window through direct imaging in living mice. ZW-MSPMs interacted strongly with important EPS components such as eDNA and protein to disperse biofilm and enhance ciprofloxacin efficacy toward remaining biofilm, both *in vitro* and *in vivo*. Zwitterionic micellar dispersants may aid infection control and enhance efficacy of existing antibiotics against remaining biofilm.

INTRODUCTION

Infectious bacterial biofilms are difficult to penetrate by antimicrobials (1, 2). Combined with the increase in antibiotic resistance in many pathogens, this forms a growing threat to public health, which has been predicted to cause antimicrobial-resistant infections to become the number one cause of human death within three decades (3). Unfortunately, at the same time, the incentives for development and marketing of new antibiotics are relatively low because the effective lifetime of new antibiotics from their first clinical use until the appearance of the first resistant bacterial strains is becoming shorter and shorter (4). This hampers return of investment of industrial endeavors needed for successful clinical translation (5). Accordingly, new strategies to complement current antibiotic treatment by existing antibiotics or even to fully replace antibiotics are direly needed to prevent this frightening scenario from becoming reality (6–8).

Biofilms are held together by a matrix composed of extracellular polymeric substances (EPS) (9, 10). The EPS matrix is self-produced by bacteria inhabiting a biofilm and constitutes a protective barrier toward penetration of antimicrobials and host immune cells (11–15). Despite the importance of the EPS matrix for protecting biofilm inhabitants and biofilm cohesivity, dispersal of biofilm inhabitants to escape a biofilm, e.g., during times of overpopulation and nutrient

scarcity, is an essential part of the biofilm life cycle (16–19). Dispersal of infectious biofilms in a human host may cause spreading of infectious bacteria within the host but is more and more regarded as a new therapeutic strategy to replace or complement antibiotic treatment because, once dispersed in the blood circulation, planktonic bacteria in suspension are more susceptible to host immune cells than bacteria in a biofilm mode of growth. Moreover, once suspended in the blood circulation, infectious bacteria are many-fold more susceptible to antibiotics than in a biofilm mode of growth (16, 20–24).

The major components in the EPS matrix responsible for keeping a biofilm together are extracellular DNA (eDNA), polysaccharides, and glycoproteins that function as a glue interacting with biofilm bacteria (15, 25, 26). A variety of bacterially produced enzymes and biosurfactants such as deoxyribonuclease (20, 27–30), dispersin B (16, 31, 32), and rhamnolipids (33–35) have been described to be responsible for natural biofilm dispersal and are also regarded for potential therapeutic use. However, bacterial enzymes and biosurfactants mostly interact with a single EPS component and are difficult to isolate, while their stability is often low. These aspects yield a need for the development of cost-effective and stable synthetic dispersants, interacting with all three major EPS components to facilitate broad clinical use.

Cationic nanoparticles are often unable to penetrate into a biofilm but accumulate at its surface (36), while anionic and neutral nanoparticles neither penetrate in nor adsorb to the biofilm and are easily rinsed out (37). Although cationic micelles can disrupt biofilms (38, 39), they lack the ability to self-target biofilm inhabitants. Mixed-shell polymeric micelles (MSPMs) composed of a poly(ethylene glycol) (PEG) shell and a pH-responsive poly(β -amino ester) have previously been demonstrated to perform very well *in vitro* and *in vivo* as antimicrobial nanocarriers, which could be transported through the blood owing to their stealth properties (40, 41). Their pH responsiveness allowed them to self-target to negatively charged bacteria in the acidic environment of *in vitro*

¹State Key Laboratory of Medicinal Chemical Biology; Key Laboratory of Functional Polymer Materials, Ministry of Education; and Institute of Polymer Chemistry, College of Chemistry, Nankai University, Tianjin 300071, P.R. China. ²University of Groningen and University Medical Center Groningen, Department of Biomedical Engineering, Antonius Deusinglaan 1, 9713 AV Groningen, Netherlands. ³University of Groningen and University Medical Center Groningen, Department of Orthodontics, Hanzplein 1, 9700 RB Groningen, Netherlands. ⁴Tianjin Key Laboratory of Radiation Medicine and Molecular Nuclear Medicine, Institute of Radiation Medicine, Chinese Academy of Medical Sciences and Peking Union Medical College, Tianjin 300192, P.R. China. *Present address: Institute of Functional Nano and Soft Materials (FUNSOM), Jiangsu Key Laboratory of Carbon-Based Functional Materials and Devices, Collaborative Innovation Center of Suzhou Nano Science and Technology, Soochow University, Suzhou 215123, China.

†Corresponding author. Email: liujianfeng@irm-cams.ac.cn (J.L.); h.c.van.der.mei@umcg.nl (H.C.v.d.M.); h.j.busscher@umcg.nl (H.J.B.); shilingqi@nankai.edu.cn (L.Sh.)

biofilms, as microscopically imaged using fluorescent micelles. However, *in vivo* targeting has only been indirectly inferred and never been directly imaged because of lack of experimental possibilities. After biofilm targeting, release of their antimicrobial cargo was stimulated by the lipase activity of biofilm bacteria, with, as a final result, the killing of biofilm inhabitants. We here demonstrate a totally new type of micelle, combining self-targeting and the ability to disrupt biofilm in one micelle. These dual-function micelles were self-assembled from PEG-*block*-poly(ϵ -caprolactone) (PEG-*b*-PCL) and PCL-*block*-poly(quaternary amino ester) (PCL-*b*-PQAE) and equipped with a zwitterionic (ZW), pH-responsive derivative of carboxybetaine having hydroxyl groups. The ZW group acted as a synthetic micellar dispersant of biofilm, interacting with eDNA and protein as the most important EPS components to interfere with their function as a glue holding biofilm bacteria together. Self-targeting was not only demonstrated *in vitro* but, uniquely, also directly imaged *in vivo* using intravital imaging (42) in living mice. To our knowledge, the use of intravital imaging in infectious biofilm research is new. Throughout this work, PEG-*b*-PCL single-shell polymeric micelles (SSPMs) were used for comparison to create a more or less comparable chemistry without the ZW feature. Use of a non-pH-sensitive zwitterion would have yielded a different chemistry.

RESULTS

Synthesis and characterization of ZW-MSPMs

An amphiphilic block copolymer PEG-*b*-PCL (43) (fig. S1A) was synthesized, as described before [see fig. S1B for ^1H nuclear magnetic resonance (NMR) spectrum], while a newly designed pH-responsive copolymer PCL-*b*-PQAE was synthesized, as schematically presented in fig. S2A. Successful synthesis of PCL-*b*-PQAE was demonstrated in the ^1H NMR spectra presented in fig. S3 (A and B). Synthesis of PCL-*b*-PQAE had a yield of 73%. Note, from the ^1H NMR spectrum in fig. S3B, that all of the bromoacetic acid was substituted. ZW PQAE changed to a lactone ring structure in trifluoroacetic acid to exhibit positive charge (fig. S2B). This conversion was monitored by ^1H NMR as a function of time (see Fig. 1A), reaching a conversion of 90% within 40 min under acidic conditions. PEG-*b*-PCL was synthesized to fabricate SSPMs for comparison. SSPMs and ZW-MSPMs were obtained by self-assembly in aqueous solution of PEG-*b*-PCL in the absence or presence of PCL-*b*-PQAE, respectively. Critical micelle concentrations (CMCs) (fig. S4) of SSPMs were slightly smaller ($1.24 \mu\text{g ml}^{-1}$) than that of ZW-MSPMs ($1.52 \mu\text{g ml}^{-1}$). ZW-MSPMs and SSPMs had comparable diameters of around 80 nm (Fig. 1, B and C). Micellar diameters were independent of pH over the pH range 5.0 to 7.4. At pH 5.0, SSPMs had a negative zeta potential of around -5 mV that remained constant in time, while ZW-MSPMs demonstrated an increase in zeta potential from -10 mV to around $+12 \text{ mV}$ after 90 to 120 min (Fig. 1D). This time dependence confirmed that the formation of a positively charged lactone ring structure is a relatively slow process, in line with the conclusion drawn from ^1H NMR. SSPM zeta potentials remained negative over the pH range 5.0 to 7.4, but the zeta potential of ZW-MSPMs became more positive upon pH decrease (Fig. 1E).

Self-targeting and antibacterial activity of ZW-MSPMs *in vitro*

In vitro, the pH responsiveness of the ZW-MSPMs allowed them to self-target up to 78% of planktonic *Staphylococcus aureus* in sus-

pension under acidic (pH 5.0) conditions, as existing in a biofilm (9). Oppositely, ZW-MSPMs at pH 7.4 self-targeted less than 11% of *S. aureus* in suspension, similar to SSPMs in pH 7.4 and 5.0 (fig. S5). Exposure of planktonic staphylococci to either ZW-MSPM or SSPM suspensions did not affect bacterial growth (fig. S6). The inability of MSPMs to self-target negatively charged bacteria at pH 7.4 *in vitro* has been amply demonstrated (40). Lack of *in vitro* self-targeting at physiological pH is confirmed here by the lack of penetration and accumulation of Nile red-loaded ZW-MSPMs over the height of an *S. aureus* biofilm at pH 7.4 versus good penetration and accumulation at pH 5.0 after short exposure times of only 30 min (Fig. 2, A and B). The distribution of green and red fluorescent pixels as a function of height at pH 5.0 overlaps (Fig. 2C), attesting the *in vitro* self-targeting of ZW-MSPMs to staphylococci, also in a biofilm mode of growth.

Intravital imaging in mice to demonstrate self-targeting of ZW-MSPMs *in vivo*

Self-targeting of smart nanocarriers has never been directly imaged *in vivo* but only indirectly inferred on the basis of a combination of *in vitro* and *in vivo* data. To directly confirm biofilm self-targeting by ZW-MSPMs *in vivo*, green fluorescent staphylococcal biofilms were grown underneath abdominal imaging windows (AIWs) in living mice (Fig. 2D) (42). An AIW uniquely allows for real-time observation of fluorescent biofilm and its targeting by fluorescent, smart nanocarriers, using a two-photon laser scanning confocal microscope. To this end, anesthetized mice were placed on the microscope stage by fixing the abdominal window frame in a clamp for intravital imaging (Fig. 2E). First, staphylococci were injected underneath the window [2×10^8 colony-forming units (CFUs) per site] to grow a biofilm for 48 hours. After 48 hours of *in vivo* growth, staphylococcal biofilm were found, using intravital imaging, to be around 70 μm thick (Fig. 2, F and G). This thickness is comparable with human clinical biofilms (44). Self-targeting of ZW-MSPMs *in vivo* was demonstrated by injection of red fluorescent Nile red-loaded SSPMs or ZW-MSPMs suspended in phosphate-buffered saline (PBS) into the tails of the mice. Subsequently, mice were held fixed on the microscope stage, and micellar targeting to the staphylococcal biofilm was real-time imaged as a function of time after injection of the micelle suspensions. SSPMs did not self-target to the biofilm (Fig. 2F), but real-time imaging demonstrated arrival of the first Nile red-loaded ZW-MSPMs in the biofilms after 20 min of blood circulation (Fig. 2G and movie S1), after which, penetration and accumulation of ZW-MSPMs in the biofilms continued (Fig. 2H). In mice without a biofilm grown underneath the intravital window, intensity of red fluorescence underneath the window was below detection (Fig. 2, F and G) after tail injection of Nile red-loaded SSPMs or ZW-MSPMs (Fig. 2, F and G).

Dispersal of biofilms by ZW-MSPMs

Next, to study dispersal of *S. aureus* biofilms by ZW-MSPMs, biofilms were exposed *in vitro* to PBS [10 mM potassium phosphate and 150 mM NaCl (pH 5.0)] and SSPMs or ZW-MSPMs suspended at different concentrations in PBS for 120 min and stained with crystal violet (CV). Loss of CV-stainable biofilm mass upon exposure to ZW-MSPM suspensions increased with increasing micelle concentration, while exposure to PBS ($0 \mu\text{g ml}^{-1}$) or SSPM suspensions yielded no loss of biomass, regardless of micelle concentration (Fig. 3A). Dispersal of *S. aureus* biofilms was also evaluated by exposing staphylococcal

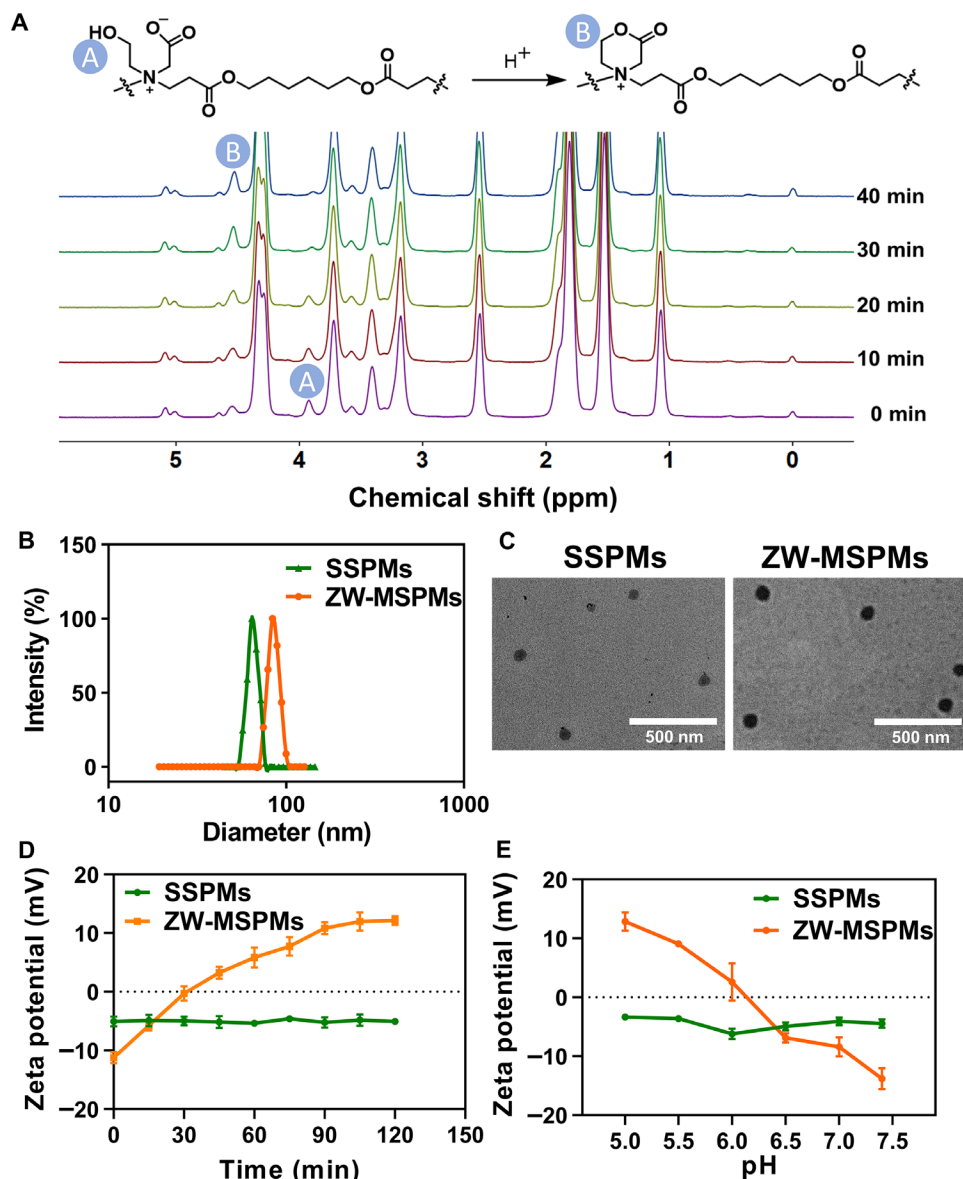


Fig. 1. Characterization of ZW-MSPMs and SSPMs prepared. (A) ^1H NMR spectra of the PQAE conversion in trifluoroacetic acid. The peak shift from A [3.92 parts per million (ppm)] to B (4.54 ppm) indicates the conversion of the ZW structure to a lactone ring structure. (B) Hydrodynamic diameter distributions of SSPMs and ZW-MSPMs at pH 7.4 in phosphate-buffered saline (PBS; 10 mM potassium phosphate and 150 mM NaCl). (C) Transmission electron microscopy (TEM) micrographs of SSPMs and ZW-MSPMs at pH 7.4. (D) Zeta potentials of ZW-MSPMs and SSPMs in PBS as a function of time measured at pH 5.0 (37°C). (E) Zeta potentials of ZW-MSPMs and SSPMs as a function of pH measured in PBS (37°C), measured after 120-min exposure to each pH. All error bars denote SDs over three separately prepared batches of micelles.

biofilms to PBS, suspended SSPMs, or ZW-MSPMs (no Nile red loading) and subsequent staining with red fluorescent concanavalin A to visualize bacteria and their EPS matrix (Fig. 3B). COMSTAT analysis (45) demonstrated that before exposure, *in vitro* staphylococcal biofilms had a thickness of $20.0 \pm 1.6 \mu\text{m}$ (Fig. 3C). Exposure to PBS or SSPM suspensions did not affect biofilm thickness and it remained at $20.0 \pm 0.8 \mu\text{m}$. However, upon exposure to ZW-MSPM suspensions, staphylococcal biofilm thickness significantly decreased to $10.0 \pm 1.4 \mu\text{m}$, confirming the results obtained after CV staining of exposed biofilms [compare Fig. 3 (A and C)]. COMSTAT was also used to derive the biomass distribution over the height of a biofilm distinguishing bacteria and EPS. Exposure to PBS yielded a similar distribution of bacterial mass

and EPS, as did exposure to an SSPM suspension (Fig. 3D). ZW-MSPM suspensions, on the other hand, caused a major loss of EPS over the height of remaining biofilm that was smaller than the corresponding heights after exposure to PBS or SSPM suspensions (see also Fig. 3D). COMSTAT analysis of biomass, separated in bacterial mass and EPS of the entire thickness of exposed biofilm, confirmed significant loss of bacterial mass and EPS upon exposure of staphylococcal biofilms to ZW-MSPM suspensions (Fig. 3E).

Interaction of ZW-MSPMs with biofilm matrix components

To find out which of the major EPS components in *S. aureus* biofilms interacted with ZW-MSPMs, the interaction of herring sperm DNA [as an eDNA mimic in the EPS matrix (46, 47)] and amyloid

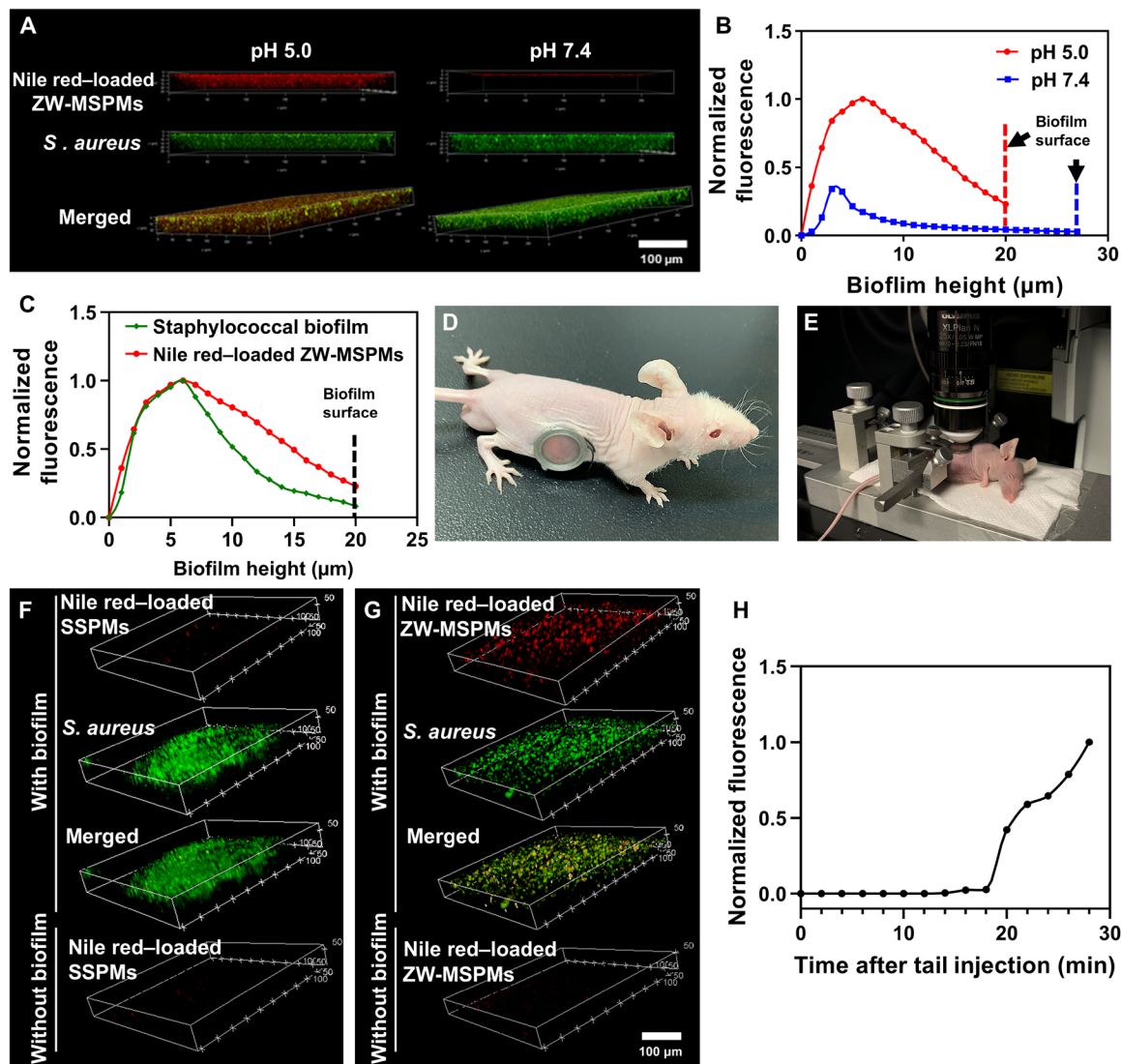


Fig. 2. Self-targeting in *S. aureus* ATCC12600^{GFP} biofilms of Nile red-loaded ZW-MSPMs in vitro and in vivo. (A) In vitro self-targeting of Nile red-loaded ZW-MSPMs into green fluorescent, 48-hour-old biofilms after 30 min of exposure to Nile red-loaded ZW-MSPMs suspended in PBS. (B) In vitro accumulation of Nile red-loaded ZW-MSPMs as a function of biofilm height. Accumulation was normalized with respect to the maximum intensity (pH 5.0). (C) Normalized green and red fluorescence as a function of biofilm height after in vitro accumulation of ZW-MSPMs at pH 5.0. Overlap of both curves indicates targeting of ZW-MSPMs to staphylococci. (D) A mouse with an abdominal imaging window (AIW) implanted in its flank underneath in which a green fluorescent staphylococcal biofilm was grown. (E) Custom-designed microscope stage, with the window frame fixed in a clamp to ensure proper intravital focusing over time. (F) Reconstructed three-dimensional (3D) intravital images of green fluorescent, 48-hour-old staphylococcal biofilms grown underneath the AIW, taken 30 min after injection of a Nile red-loaded SSPM suspension in PBS (pH 7.4). The bottom intravital image is the red fluorescence channel, taken 30 min after injection of a Nile red-loaded SSPM suspension in mice without a staphylococcal biofilm grown underneath the window. (G) Same as (F), demonstrating in vivo accumulation of red fluorescent ZW-MSPMs in the 48-hour-old biofilm. (H) Red fluorescence intensity due to Nile red-loaded ZW-MSPMs accumulated in a 48-hour-old biofilm underneath the window as a function of time after tail injection of micelles. Intravital images were taken every 2 min. In three mice, without a biofilm grown underneath the window, no detectable red fluorescence due to micelle accumulation was observed. Red fluorescence intensity was normalized with respect to the maximum intensity after 28 min. Photo credit: (D and E) Shuang Tian, Nankai University and University Medical Center Groningen.

fibrils [endogenous to *S. aureus* biofilms (48–50)] with ZW-MSPMs was investigated using different in vitro methods. In an acidic environment, positively charged ZW-MSPMs in PBS (pH 5.0) interacted significantly better with DNA (Fig. 4A) and proteinaceous amyloid fibrils (Fig. 4B) than SSPMs. EPS remained clearly visible in biofilms after exposure to PBS or SSPM suspensions (Fig. 4C). After exposure to ZW-MSPM suspensions, all traces of the EPS matrix components were removed from the remaining

staphylococcal cell surfaces (Fig. 4C). This points to a stronger interaction between ZW-MSPMs with staphylococci than between EPS matrix components and staphylococci. Thus, interactions between ZW-MSPMs and staphylococci will impede or break interactions between matrix components and bacterial inhabitants within a biofilm and, therewith, negatively affect biofilm integrity to yield dispersal.

One of the main causes of biofilm resistance to antibiotics is that the EPS matrix prevents the penetration of antibiotics. ZW-MSPMs

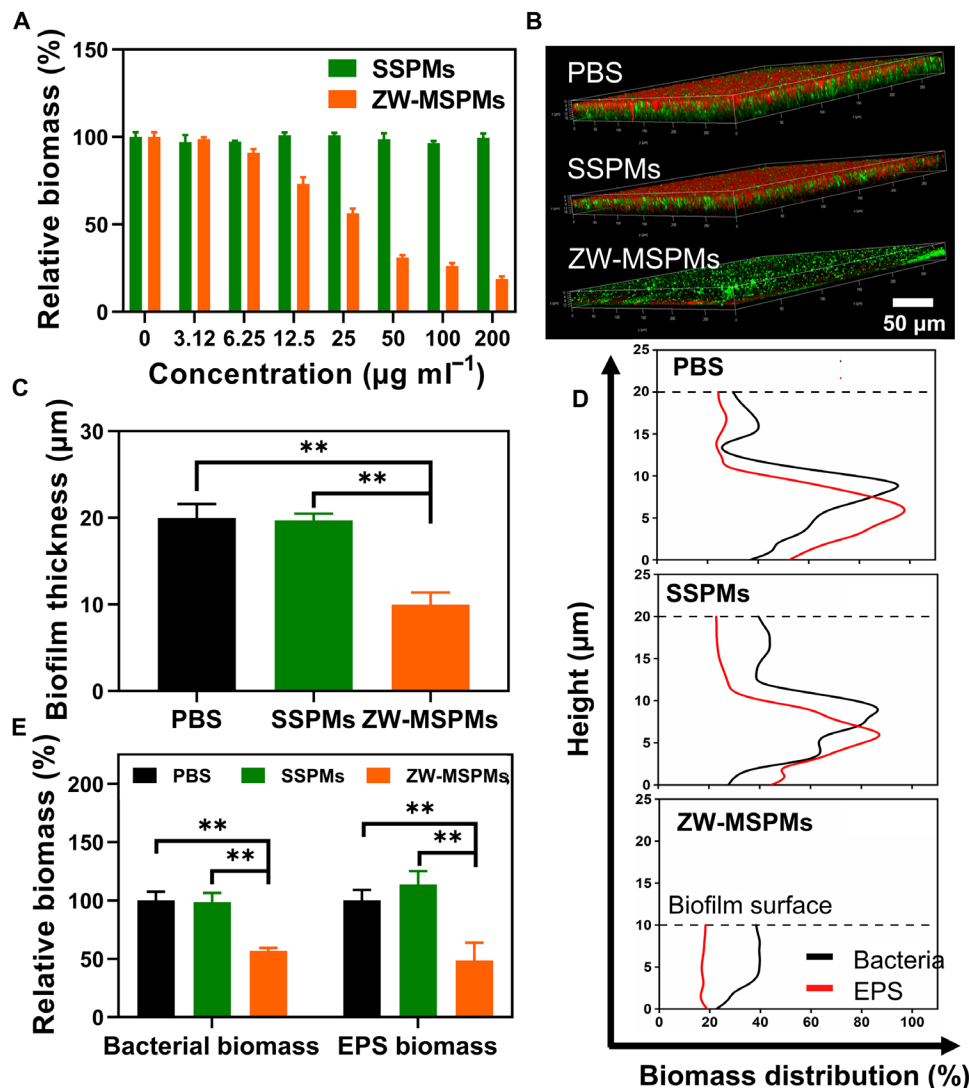


Fig. 3. Dispersal of 48-hour-old *S. aureus* ATCC12600^{GFP} biofilms upon 120 min of exposure to ZW-MSPMs or SSPMs in PBS (pH 5.0). (A) CV-stainable bacterial biomass relative to PBS (pH 5.0), derived from optical density at 595 nm (OD_{595nm}) after CV staining of in vitro-grown *S. aureus* biofilms as a function of micelle concentration in suspension. (B) Confocal laser scanning microscopy (CLSM) micrographs of staphylococcal biofilms exposed to PBS or suspensions ($200 \mu\text{g ml}^{-1}$) of SSPMs and ZW-MSPMs. (C) Thickness of staphylococcal biofilms after exposure to PBS or suspensions of SSPMs or ZW-MSPMs. (D) Example of biomass distribution after exposure to PBS, or suspensions ($200 \mu\text{g ml}^{-1}$) of SSPMs and ZW-MSPMs, across the height of the staphylococcal biofilms. Bacterial biomass was derived from green fluorescent pixels, while EPS mass was derived from red fluorescent pixels. Maximal green and red fluorescence intensities after exposure were set to 100%. (E) Biomass relative to PBS of bacteria and EPS, derived from COMSTAT analysis of CLSM images of staphylococcal biofilms exposed to micellar suspensions [micelles ($200 \mu\text{g ml}^{-1}$)]. All error bars denote SDs over three experiments with separately prepared micelle batches and differently grown staphylococcal cultures. ** denotes statistically significant differences at $P < 0.01$ (Student's *t* test).

were shown here to disperse a staphylococcal biofilm, although roughly half of a staphylococcal biofilm was remaining (Fig. 3, C and E). However, because of reduced presence of EPS-induced coherence of the biofilm (Fig. 4C), the remaining biofilm after exposure to ZW-MSPM suspensions was easier to penetrate by ciprofloxacin, a common antibiotic in the clinical treatment of staphylococcal infections (Fig. 5, A and B), than when exposed to PBS or SSPM suspensions. Moreover, whereas the biofilm thickness (Fig. 3C) and biomass (Fig. 3E) were reduced twofold upon exposure to ZW-MSPM suspensions compared to PBS and SSPM suspensions, staphylococcal killing increased four log units of CFUs (Fig. 5,

C and D). Thus, it can be concluded that pre-exposure of biofilms to ZW-MSPM suspensions enhanced bacterial killing by antibiotics, with a clear impact of antibiotic concentration (see also Fig. 5C).

Effect of biofilm dispersal by ZW-MSPMs on antibiotic efficacy in vivo

In a second series of in vivo experiments, an infectious biofilm grown underneath an AIW was imaged during consecutive injection of micelles and ciprofloxacin. Ciprofloxacin was injected in the tails of the mice, immediately after tail injection of PBS, SSPMs or ZW-MSPMs suspended in PBS at pH 7.4 (see scheme in Fig. 6A).

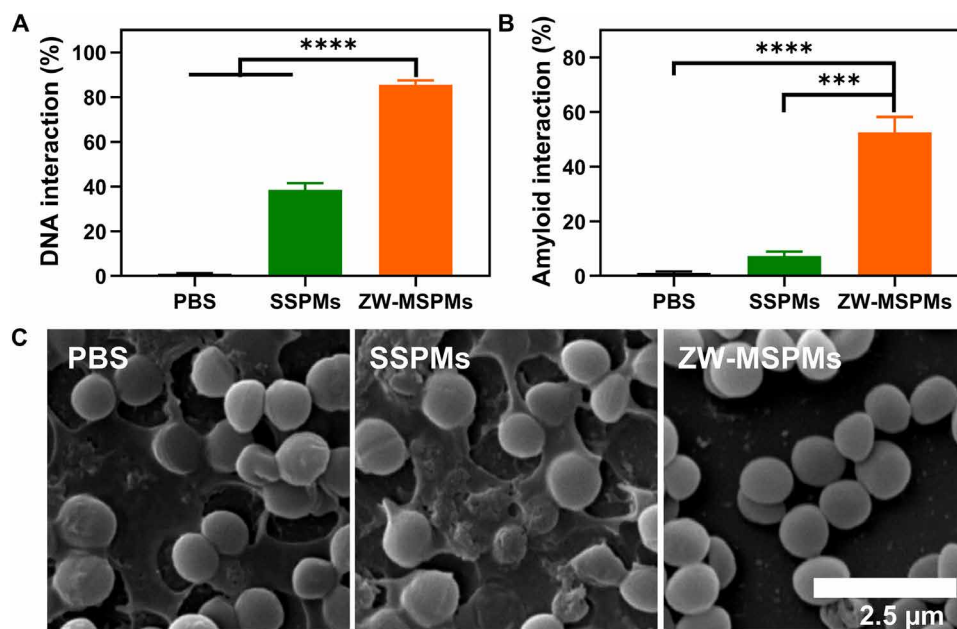


Fig. 4. Interactions of SSPMs or ZW-MSPMs suspended in PBS (pH 5.0) with two major staphylococcal EPS components and effects on a 48-hour-old biofilm (scanning electron microscopy). (A) Effects of exposure of DNA for 120 min to PBS or suspensions ($200 \mu\text{g ml}^{-1}$) of SSPMs or ZW-MSPMs. DNA interaction was assessed by an ethidium bromide (EB) displacement assay, with 100% coinciding with full displacement of EB. (B) Same as (A), for interaction with proteinaceous amyloid fibrils. Amyloid interaction was assessed by a thioflavin T (ThT) fluorescence assay, with 100% coinciding with full disruption of amyloid fibrils. Error bars denote SDs over three experiments with separately prepared micelle batches. *** and **** indicate statistically significant differences at $P < 0.001$ and $P < 0.0001$, respectively (Student's *t* test). (C) Scanning electron microscopy (SEM) images of 48-hour-old *S. aureus* ATCC12600^{GFP} biofilms after 120 min of exposure to PBS or suspensions ($200 \mu\text{g ml}^{-1}$) of SSPMs and ZW-MSPMs, demonstrating EPS patches in biofilms exposed to PBS and SSPMs but not after exposure to ZW-MSPMs.

The green fluorescent staphylococcal biofilm remained clearly observable upon pretreatment with tail injection of PBS or an SSPM suspension followed by ciprofloxacin injection for at least 5 days. However, when a ZW-MSPM suspension was applied in combination with subsequent ciprofloxacin injection, the infectious biofilm entirely disappeared over the course of 3 to 5 days (Fig. 6B). Biofilm thickness and biomass decreased as a function of time after injection [Fig. 6 (C and D, respectively)], most notably after tail injection of a ZW-MSPM suspension and ciprofloxacin. After sacrifice, the surrounding tissue excised from the infection site harvested a four log unit–larger reduction in CFUs (CFUs/site) after pretreatment with a ZW-MSPM suspension followed by ciprofloxacin than when PBS or a SSPM suspension was applied as a pretreatment (Fig. 6E). Eradication of the infectious staphylococci at sacrifice due to pretreatment with a ZW-MSPM suspension followed by ciprofloxacin injection was confirmed by enumeration of white blood cells and neutrophilic granulocytes in blood after sacrifice, a key parameter to indicate the status of bacterial infection (51, 52). Five days after pretreatment with a ZW-MSPM suspension and ciprofloxacin injection, white blood cell counts were back to normal and granulocyte counts were almost back to normal, while highly elevated immune cell counts were still found in the blood of mice pretreated with PBS or a SSPM suspension (fig. S7). Concentrations of other blood markers were all within the range observed for uninfected mice (fig. S8), indicating the absence of adverse blood reactions, for both SSPM and ZW-MSPM suspensions. No indications were found of micelle collection in or damage to the major organs, as can be concluded from histological images of the heart, liver, spleen, lung, and kidney (fig. S9).

DISCUSSION

In conclusion, this work describes the synthesis of new self-targeting ZW-MSPMs as a synthetic biofilm dispersant. Use as a dispersant is an entirely new application of MSPMs. When equipped with ZW and pH-responsive PQAE and PEG, ZW-MSPMs had the ability to interact strongly with major components (eDNA and protein) of the EPS matrix of staphylococcal biofilms to disrupt the interaction between bacterial inhabitants with the EPS matrix and, therewith, the cohesivity of the biofilm, yielding its dispersal. Uniquely, micellar self-targeting toward an infectious biofilm was observed real time in living mice underneath an AIW implanted in their flanks, providing the first direct evidence of self-targeting through the blood circulation of tail-injected ZW-MSPMs toward an infectious biofilm in mice (Fig. 2, F and G). None of other self-targeting, pH-responsive nanocarriers described in the literature (24–30) have yet been directly demonstrated to be able to find their own highway through the body of a living animal toward an infection site. This shows the great potential of intravital imaging for demonstration of proof of principle. In line with the recommendations of an international consortium (53), suggesting to solely conduct animal experiments for preclinical proof of principle and safety, we relied on *in vitro* models to explore mechanisms of action of our ZW-MSPMs. In addition, although the morbidity of placing an AIW is unexpectedly low, possibly comparable with the inconvenience encountered by patients with intestinal stoma, we limited animal use to three animals per group, as also suggested by the international consortium (53).

Pretreatment of an existing staphylococcal biofilm with ZW-MSPM suspensions made the remaining biofilm more susceptible to

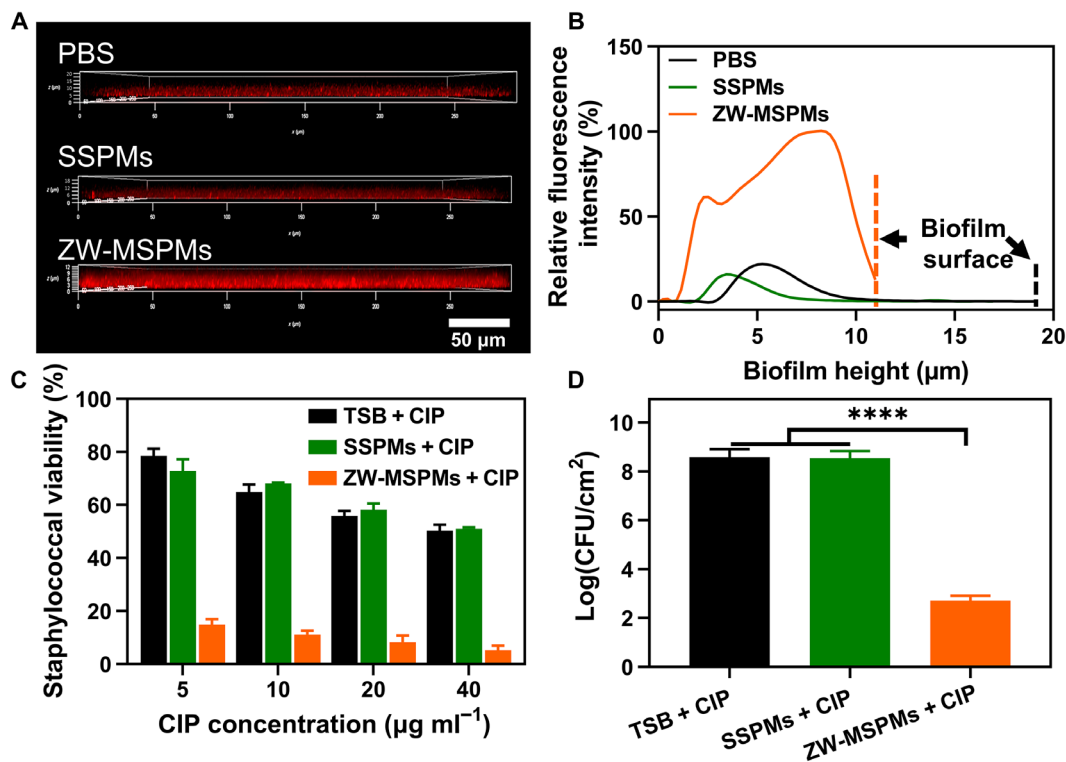


Fig. 5. Antibiotic effects on 48-hour-old *S. aureus* ATCC12600^{GFP} biofilm remaining after dispersal by exposure to ZW-MSPMs or SSPMs suspended in PBS (pH 5.0). (A) CLSM images of the penetration of red fluorescent ciprofloxacin (CIP) in in vitro-grown *S. aureus* biofilms after 120 min of exposure to PBS or suspensions (200 μg ml⁻¹) of SSPMs or ZW-MSPMs. (B) Red fluorescence due to ciprofloxacin penetration, as a function of height in staphylococcal biofilms, derived from CLSM images (A). (C) Viability of staphylococci in a biofilm mode after pre-exposure to TSB or suspensions (200 μg ml⁻¹) of SSPMs and ZW-MSPMs for 120 min and subsequent exposure to various concentrations of ciprofloxacin in TSB for 5 hours. Staphylococcal viability was assessed from the green fluorescence of the biofilms. Green fluorescence of biofilms before ciprofloxacin exposure was set to 100%. (D) Number of *S. aureus* colonies formed per square centimeter well surface in a biofilm mode, pre-exposed to tryptone soya broth (TSB) or suspensions (200 μg ml⁻¹) of SSPMs and ZW-MSPMs for 120 min and subsequently exposed to ciprofloxacin (40 μg ml⁻¹) for 5 hours. Error bars denote SDs over three experiments with separately prepared micelle batches and differently grown staphylococcal cultures. **** indicates statistically significant differences at $P < 0.0001$ (Student's *t* test).

ciprofloxacin penetration and killing of its inhabitants than pretreatment with PBS or SSPM suspensions, both in vitro and in vivo. Staphylococcal biofilms grown in mice underneath an AIW fully disappeared within 5 days after pretreatment with a ZW-MSPM suspension followed by ciprofloxacin injection, while undispersed biofilm remained clearly observable when SSPMs were applied (Fig. 6). Although, a priori, there are no reasons to assume that the ZW micellar dispersants prepared will not work on biofilms grown from other infectious bacterial strains and species, we have also determined the interaction of the ZW-MSPMs with alginate, an important EPS component in Gram-negative pseudomonas biofilms. ZW-MSPMs also demonstrated a strong interaction with alginate (fig. S10). Thus, it can be expected that our dual-function ZW-MSPMs will show disperse infectious biofilms of other pathogens, but this remains to be confirmed. Similarly, although within reason to expect, enhanced antibiotic efficacy in combination with our micellar dispersants should also be confirmed for other antibiotics.

In mice, no adverse effects were observed of the dual-function ZW-MSPMs, paving the way to clinical application. With respect to clinical application of our micellar dispersants, synthetic ZW micellar dispersants are cheap and easy to manufacture. ZW-MSPMs in combination with existing antibiotics aid infection control by enhancing the efficacy of antibiotic treatment. However,

they may also aid infection control without their combination with existing antibiotics. This is because dispersed bacteria are more easily cleared from the blood circulation by immune cells than bacteria in a biofilm mode of growth (16). However, before possible stand-alone use, it may be considered advantageous that clinical trials can be carried out by combining existing antibiotics with our synthetic ZW dispersants. In a first instance, this might be done for easy-to-treat infections and slowly progressing to more serious hard-to-treat antibiotic-resistant infections. Such a step-by-step approach likely will be more acceptable for clinical trials than an approach in which a seriously infected patient is from the onset made 100% dependent on a novel therapy.

MATERIALS AND METHODS

Materials

Monomethoxy PEG (CH₃O-PEG-OH; $M_w = 2000$) was purchased from Fluka (Shanghai, China) and dried under vacuum before use. ε-Caprolactone (ε-CL; 99% purity), purchased from Alfa Aesar (Shanghai, China), was dried with calcium hydride and was subsequently distilled under vacuum conditions. Stannous octoate [Sn(Oct)₂; 95% purity] was purchased from J&K (Beijing, China) and used as received. All other materials and solvents were used as

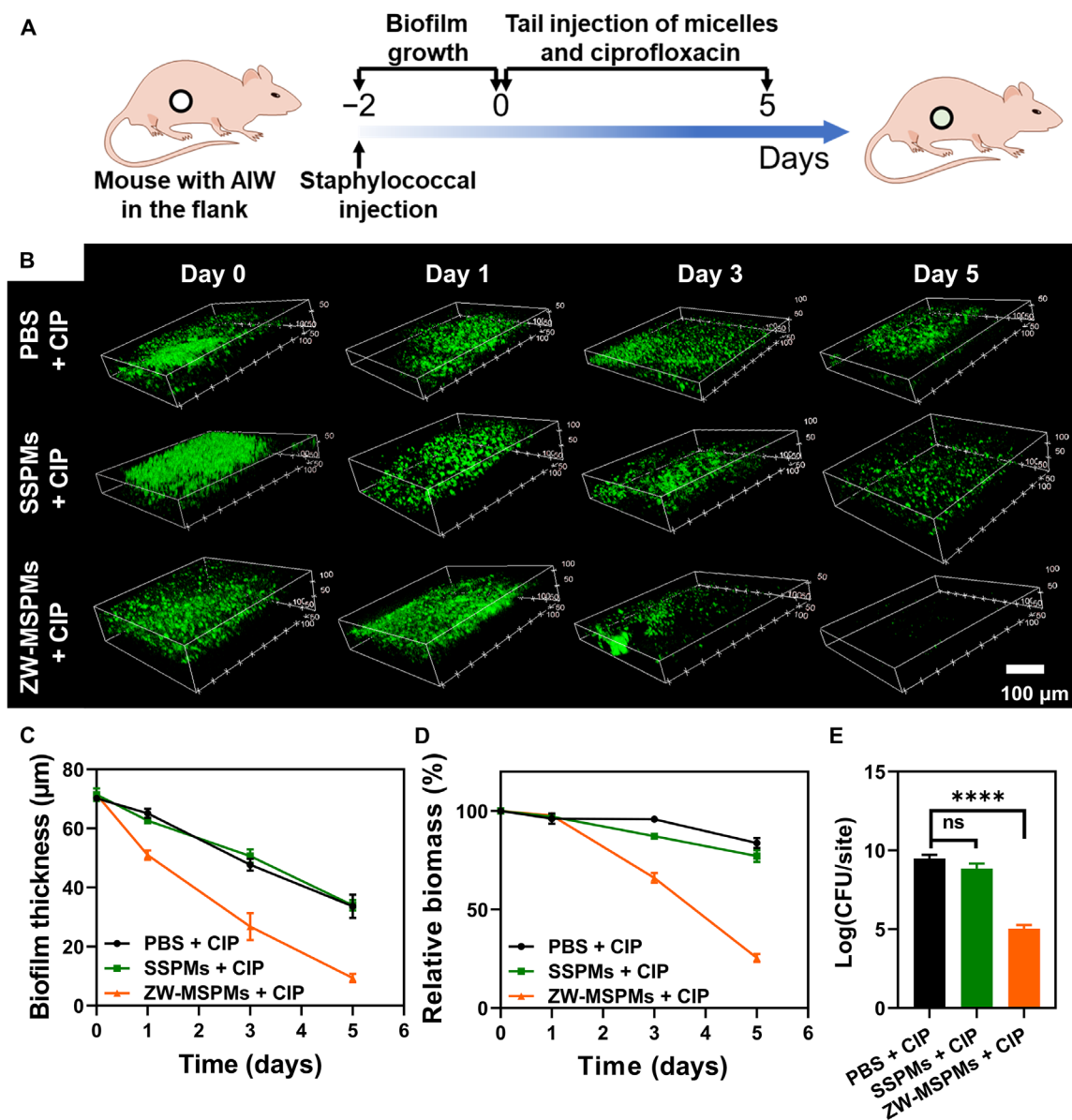


Fig. 6. In vivo efficacy of antibiotic treatment of an infectious *S. aureus* ATCC12600^{GFP}, pretreated with ZW-MSPMs or SSPMs. (A) Experimental scheme for experiments using intravital imaging in mice equipped with an AIW. Consecutive tail injections of micelles and ciprofloxacin were performed daily, starting at day 0, i.e., 48 hours after initiating growth of an infectious biofilm (day –2). Injection with PBS, SSPMs, or ZW-MSPMs was immediately followed by injection of ciprofloxacin. **(B)** Reconstructed 3D intravital images of green fluorescent *S. aureus* biofilms before treatment at day 0 and after tail injection of PBS or SSPMs and ZW-MSPMs suspended in PBS (pH 7.4; 200 μg ml⁻¹), immediately followed by ciprofloxacin in PBS (1 mg ml⁻¹). Images were taken at different days up to sacrifice at day 5. **(C)** Thickness of staphylococcal biofilms underneath the AIW as a function of time after initiating treatment, derived from COMSTAT analysis of intravital images. **(D)** Same as (C), now for biomass. **(E)** Number of *S. aureus* CFUs obtained from the AIW and infection site tissue excised after sacrifice at day 5. Error bars denote SDs over three mice. **** indicates statistically significant differences at $P < 0.0001$ (Student's *t* test). ns, not significant.

received without further purification from commercial suppliers, with the exception of chloroform (CHCl₃), which was dried over calcium hydride and distilled before use. All aqueous solutions were prepared with ultrapure water (resistance, >18 megohm cm⁻¹) from a Millipore Milli-Q system.

Synthesis of block copolymers

PEG-*b*-PCL was synthesized as shown in fig. S1A, as previously described (43). ¹H NMR identified the polymer prepared as PEG₄₅-*b*-PCL₄₂ (fig. S1B). The number-average molecular weight

(M_n) and the polydispersity index (M_w/M_n , in which M_w is the weight-average molecular weight) of PEG-*b*-PCL amounted to 7930 and 1.28, respectively, as determined by gel permeation chromatography at 35°C on a Waters 1525 chromatograph equipped with a Waters 2414 refractive index detector. Tetrahydrofuran was used as eluent at a flow rate of 1 ml min⁻¹. Polystyrene standards were used for calibration.

PCL-*b*-PQAE was synthesized by a Michael-type addition polymerization of PCL monoacrylate, hexane-1,6-dioldiacrylate (HDD), and ethanolamine (fig. S2A). To obtain PCL monoacrylate,

2-hydroxyethyl acrylate (0.093 g, 0.8 mmol) and ϵ -CL (5.0 g, 43.8 mmol) was dissolved in 15 ml of toluene, after which one drop of Sn(Oct)₂ was added into the solution. After three freeze-degas-thaw cycles, the reaction mixture was stirred at 110°C for 12 hours. Next, the solvent was precipitated into excess diethyl ether to obtain the crude product. The PCL monoacrylate was dried under vacuum. ¹H NMR identified the degree of polymerization of the PCL monoacrylate prepared as 44 (fig. S3A). PCL monoacrylate (2.5 g, 0.5 mmol), HDD (3.959 g, 17.5 mmol), and ethanolamine (1.099 g, 18 mmol) were carefully weighed and dissolved into 15 ml of anhydrous CHCl₃ in a round-bottom flask. Polymerization was performed at 55°C under a dry argon atmosphere for 72 hours. Subsequently, excess bromoacetic acid (3.75 g, 27 mmol) was added into the mixed solution and stirred for 24 hours to yield PCL-*b*-PQAE. Then, the mixture was precipitated with an excess of cold diethyl ether. The precipitate was dried under vacuum, and a pale-yellow solid product was obtained with a yield of 73%. ¹H NMR identified the polymer prepared as PCL₄₄-*b*-PQAE₂₀ (fig. S3B). *M_n* was 11,500, while the polydispersity index *M_w*/*M_n* was 1.33.

Micelle preparation and characterization

Micelles were prepared through nanoprecipitation. Briefly, PEG-*b*-PCL and PCL-*b*-PQAE were dissolved in dimethyl sulfoxide as stock polymer solution with a concentration of 5 mg ml⁻¹. For the preparation of ZW-MSPMs, 1 ml in PEG-*b*-PCL stock solution was mixed with 1 ml of PCL-*b*-PQAE stock solution, with an equal weight ratio of PEG-*b*-PCL and PCL-*b*-PQAE (1:1). The resulting solution was added dropwise to 6 ml of deionized water at 30-s intervals under vigorous stirring with a magnetic bar. After stirring for 2 hours, the micelle solution was transferred to a dialysis bag (molecular weight cutoff, 3500) and dialyzed against PBS [10 mM potassium phosphate and 150 mM NaCl (pH 7.4)] for 2 days, followed by ultrafiltration to remove all precipitation. The SSPMs composed of only PEG-*b*-PCL (SSPMs) were prepared essentially the same as the preparation of ZW-MSPMs, the only difference being that PEG-*b*-PCL in dimethyl sulfoxide was used.

Dynamic light scattering to determine the micelle diameters was done at a 90° scattering angle at 37°C with a 636-nm laser light scattering spectrometer (BI-200SM), equipped with a digital correlator (BI-10000AT). Zeta potentials of the micelles were measured in PBS at pH 5.0 as a function of time and as a function of pH (5.0 to 7.4) after 120-min exposure to each pH using a Brookhaven ZetaPALS (Brookhaven Instrument, USA). The instrument uses phase analysis scattered light at 37°C to provide an average zeta potential over multiple particles. Zeta potentials were measured in triplicate with separate batches of micelles. Micelle morphology was observed using transmission electron microscopy (TEM; Talos F200C, FEI, USA) at an acceleration voltage of 200 kV. Samples were prepared for TEM by dropping a micelle suspension onto a carbon-coated copper grid and slow drying in vacuo at room temperature.

To determine the CMC of SSPMs and ZW-MSPMs, pyrene was used as a fluorescence probe. The fluorescence intensity ratio between the first vibration peak at 373 nm and the third one at 384 nm (*I*₃₇₃/*I*₃₈₄) in the fluorescence emission spectrum of pyrene strongly depends on the polarity of the environment to which it is exposed. Accordingly, the CMC of a suspension can be determined by the change in fluorescence intensity ratio after dissolving pyrene in a micelle suspension (54). To this end, pyrene was dissolved in

acetone at a concentration of 0.6 mM. Ten-microliter aliquots of the pyrene solution were added into 1.5-ml Eppendorf centrifuge tubes, and the acetone was allowed to evaporate overnight. Next, 450 μl of micelle suspensions diluted in deionized water to different concentrations were added into the centrifuge tubes. The tubes were shaken overnight on a dry bath incubator in the dark. Fluorescence emission spectra were recorded using a fluorescence spectrometer (Hitachi F-4600, Tokyo, Japan) at an excitation wavelength of 334 nm. The emission spectrum was monitored for wavelengths between 350 and 500 nm. The fluorescence intensity ratio *I*₃₇₃/*I*₃₈₄ was used to indicate CMC (fig. S4).

Staphylococcal culturing and harvesting

Green fluorescent protein (GFP) expression in *S. aureus* ATCC12600 (American Type Culture Collection, USA) pMV148 GFP was generated, as described before (55). *S. aureus* ATCC12600^{GFP} was grown, as described before (40). Briefly, the strain was cultured from a frozen stock onto tryptone soy agar plates [tryptone soya broth (TSB); Oxoid, Basingstoke, UK] supplemented with tetracycline (10 μg ml⁻¹) at 37°C in ambient air. For experiments, one colony was transferred to inoculate 10 ml of TSB, also supplemented with tetracycline (10 μg ml⁻¹) at 37°C for 24 hours in ambient air. This preculture was diluted 1:20 in 100 ml of TSB and grown statically for 16 hours at 37°C. Cultures were harvested by centrifugation for 5 min at 5000g at 10°C, washed twice in PBS, sonicated for 3 × 10 s (Vibra-Cell model 375; Sonics and Materials Inc., Danbury, CT) while cooling in an ice/water bath to break bacterial aggregates, and lastly suspended in 10 ml of PBS to a concentration of 3 × 10⁸ bacteria ml⁻¹, as determined in a Bürker-Türk counting chamber.

Interaction of micelles with planktonic staphylococci

To demonstrate the interaction of the micelles with planktonic staphylococci, red fluorescent Nile red was entrapped inside the micelle core, as described before (40). Briefly, Nile red was dissolved in dimethylformamide (500 μl, 1 mg ml⁻¹) and added dropwise to the polymer solution from which micelles were prepared, as described above. This procedure yielded Nile red-loaded micelles.

Nile red-loaded SSPM or ZW-MSPM suspensions (500 μg ml⁻¹) were mixed with 1 ml of a *S. aureus* ATCC12600^{GFP} (3 × 10⁸ bacteria ml⁻¹) suspended in PBS at pH 7.4 or 5.0 in a sterile 20-mm glass-bottom confocal dish. After 90 min at 37°C, the PBS was removed, and wells were washed twice with PBS. Micrographs were taken with confocal laser scanning microscopy (CLSM; TCS SP8, Leica, Wetzlar, Germany). Each assay was carried out in triplicate with separate bacterial cultures. All data were acquired and analyzed using Leica software version 2.0 and ImageJ software.

Penetration and accumulation of micelles in staphylococcal biofilms

To investigate the penetration and accumulation of micelles in staphylococcal biofilms, 1 ml of a staphylococcal suspension (3 × 10⁸ bacteria ml⁻¹) was placed in a sterile 20-mm, confocal, glass-bottom dish for 1.5 hours at 37°C to allow bacteria to adhere. Next, dishes were carefully washed three times in buffer to remove planktonic bacteria. Then, TSB medium was added into the dishes and incubated at 37°C, refreshing medium every 24 hours to allow biofilm growth. After 48 hours, the biofilms were rinsed three times with PBS to remove planktonic bacteria and exposed to

Nile red-loaded ZW-MSPMs suspended in PBS at pH 7.4 or 5.0 ($200 \mu\text{g ml}^{-1}$). After 0.5 hours, exposed biofilms were rinsed three times with buffer and observed using CLSM to visualize penetration and accumulation of red fluorescent micelles into green fluorescent biofilm. Each experiment was carried out in triplicate with separately grown biofilms. All data were acquired and analyzed using Leica software version 2.0 and ImageJ software to yield biofilm thickness before and after exposure to micelles and micelle penetration and accumulation.

Bacteria and EPS in staphylococcal biofilms before and after exposure to micelle suspensions

To distinguish between green fluorescent staphylococci and EPS in biofilms, separately grown biofilms were exposed to SSPMs or ZW-MSPMs suspended in PBS at pH 5.0 ($200 \mu\text{g ml}^{-1}$) for 120 min in the absence of Nile red loading and stained with tetramethylrhodamine conjugate of concanavalin A, yielding red fluorescence of the EPS matrix. CLSM analysis, as described above, complemented with COMSTAT 2 analyses allowed computer-assisted distinction between bacteria and EPS in the staphylococcal biofilms.

Determination of staphylococcal biofilm dispersal by micelle suspensions

To determine the biofilm mass before and after exposure to SSPMs or ZW-MSPMs suspended in PBS at pH 5.0 ($200 \mu\text{g ml}^{-1}$) for 120 min, subsequently, 500 μl of a CV solution (1%, w/v) was added to each well to stain the biofilms for 20 min. Next, CV solution was removed, and wells were gently rinsed three times with PBS. After rinsing, 500 μl of 33% acetic acid was added to resuspend the stained biofilm for 15 min and absorbance in each well was read on a microplate reader (Spark, Tecan, Switzerland) at 595 nm. Each assay was carried out in triplicate with separately grown biofilms.

For scanning electron microscopy (SEM) analysis, biofilms were cultured on glass slides in 24-well plates, as described above. After exposure to PBS or suspensions ($200 \mu\text{g ml}^{-1}$) of SSPMs or ZW-MSPMs for 120 min, the biofilms were washed three times with PBS and then fixed with 2.5% glutaraldehyde for 2 hours at 4°C. After fixation, samples were dehydrated with a series of ethanol solution. Last, the samples were disposed by metal spraying and observed using Quanta 200 SEM (FEI, Hillsboro, OR, USA).

Planktonic growth of *S. aureus* in the presence of micelles

To determine the effect of SSPMs and ZW-MSPMs on staphylococcal growth, 100 μl of a bacterial culture [optical density at 600 nm (OD_{600}) = 0.1] was added into 96-well plates. Optical densities of the bacterial suspensions were measured using a UV-1800 ultraviolet-visible spectrophotometer (Shimadzu, Tokyo, Japan). Then, staphylococci were mixed with an equal volume of a micelle suspension in TSB and incubated at 37°C. Growth of planktonic staphylococci in each well was assessed by determining the OD_{600} using a microplate reader at different micelle concentrations in suspension (fig. S6). Each assay was carried out in triplicate with separate bacterial cultures.

Interaction of EPS components with ZW-MSPMs

To explore interaction of ZW-MSPMs with eDNA and proteins as the two major components in staphylococcal EPS, herring sperm DNA and proteinaceous amyloid fibrils were used to simulate the respective EPS components. To investigate the interaction between

ZW-MSPMs and DNA, 2 μg of ethidium bromide (EB) was dissolved in PBS (1 ml; pH 7.4 or 5.0). The fluorescence of the solution was measured at an excitation wavelength of 212 nm and emission at 590 nm using a spectrometer. Then, 10 μg of DNA was added into the EB solution to bind to the DNA, and subsequently, fluorescence was recorded after 30 min. Suspensions of SSPMs or ZW-MSPMs in PBS ($200 \mu\text{g ml}^{-1}$) were added into the EB-DNA solution to obtain series with different micelle/DNA ratios. Suspensions were mixed to allow micelles to disrupt EB-DNA complexes, and fluorescence was measured. Upon interaction between micelles and DNA, EB is displaced, causing a fluorescence reduction. DNA interaction with micelles was subsequently expressed as relative fluorescence calculated as

$$\text{DNA interaction} = \left(1 - \frac{I - I_{\text{EB}}}{I_{\text{EB/DNA}} - I_{\text{EB}}}\right) \times 100\% \quad (1)$$

in which I is the fluorescence intensity of the EB-DNA solution mixed with micelles, I_{EB} is the fluorescence intensity of EB solution, and $I_{\text{EB/DNA}}$ is the fluorescence intensity of the DNA and EB solution. Accordingly, full displacement of EB, i.e., maximal interaction of micelles with DNA, corresponds with 100%. Each assay was carried out in triplicate.

To investigate the interaction between proteins and ZW-MSPMs, a thioflavin T (ThT) amyloid fibril assay was performed. Five hundred microliters of ThT (26 μM) was added to a well after biofilm growth and exposure to micelles for 120 min. Subsequently, ThT was removed and 1 ml of PBS was added and pipetted vigorously in each well to detach the remaining biofilms and to homogenize the samples. Fluorescence in each well was measured using an excitation wavelength of 440 nm and emission at 485 nm on a microplate reader. Micelle interaction with amyloidosis proteins was calculated as

$$\text{Amyloid interaction (\%)} = \frac{I_0 - I}{I_0} \times 100\% \quad (2)$$

in which I_0 is the ThT fluorescence of biofilm before micelle exposure and I is the ThT fluorescence of biofilm after micelle exposure. Accordingly, maximal interaction of amyloidosis proteins was 100%. Each assay was carried out in triplicate.

Penetration and accumulation of ciprofloxacin in staphylococcal biofilms after pre-exposure to ZW-MSPMs in vitro

To investigate the penetration of antibiotics in staphylococcal biofilms in vitro after pre-exposure to PBS, SSPMs, or ZW-MSPMs suspended in PBS at pH 5.0 ($200 \mu\text{g ml}^{-1}$) for 120 min, biofilms were subsequently exposed to red fluorescent cyanine 5 (CY5)-conjugated ciprofloxacin ($40 \mu\text{g ml}^{-1}$) for 30 min and observed using CLSM to visualize penetration of red fluorescent antibiotics into green fluorescent biofilm. All data were acquired and analyzed using Leica software version 2.0 and ImageJ software. Penetration of CY5-conjugated antibiotics was calculated relative to the highest red fluorescence pixel intensity in an image. Each assay was carried out in triplicate.

Antibiotic killing of staphylococci in their biofilm mode of growth after pre-exposure to ZW-MSPM suspensions in vitro

Biofilms were cultured in 24-well plates, as described above. After pre-exposure to TSB, SSPMs, or ZW-MSPMs suspended in TSB ($200 \mu\text{g ml}^{-1}$) for 120 min, biofilms were washed three times with

PBS and exposed to various concentrations of ciprofloxacin for 5 hours. The viability of the bacteria was assessed from the fluorescence intensity of *S. aureus* ATCC12600^{GFP} biofilms on a microplate reader. Fluorescence intensity immediately after ciprofloxacin exposure was set to 100%. In addition, after pre-exposure followed by exposure to ciprofloxacin at a concentration of 40 $\mu\text{g ml}^{-1}$ for 5 hours, biofilms were scraped off a well and staphylococci was suspended in PBS (pH 7.4). The suspensions were serially diluted with PBS, and 50 μl of each dilution was plated on TSB agar and incubated at 37°C. After 24 hours, the number of CFUs per square centimeter well plate was calculated as a measure of staphylococcal viability, assuming homogeneous distribution of bacteria across a biofilm. The experiments were done in triplicate with separately grown biofilms.

Implantation of an AIW in mice

Four- to five-week-old healthy female BALB/c nude mice were obtained from Vital River Laboratories (Beijing, China) and subjected to experiments in accordance with the Guidelines for Care and Use of Laboratory Animals of Nankai University. Experiments were approved by the Animal Ethics Committee of Nankai University (Tianjin, China). Nude mice were used, as they are relatively vulnerable to bacterial infections and therefore used in many evaluations of new infection-control strategies (41, 56, 57). AIWs were implanted (42) under anesthesia. For anesthesia, an aqueous solution of 4 weight % chloral hydrate (8.25 ml/kg) was injected in the abdominal cavity of each mouse and right flanks were disinfected with 70% (v/v) ethanol. Chloral hydrate was used for anesthesia, as chloral hydrate anesthesia lasts relatively long, as required for intravital imaging. To avoid abdominal irritation, chloral hydrate was used at a low concentration, below the concentration, causing abdominal irritation (58, 59). Next, a lateral incision was made through the skin and abdominal wall, and a suture was sewed along the edge of the wound. A sterilized AIW (circular coverslips, 12 mm in diameter; Thermo Scientific, Waltham, MA, USA) in a titanium frame was placed glass side up in the incision. The skin and the abdominal wall were placed in a slot, prepared in the side of the titanium frame. Last, sutures were then tightened to secure the window frame firmly in the animal. After the surgery, the mice were kept at 37°C until fully recovered. After full recovery, usually requiring 2 days, mice were anaesthetized and injected with green fluorescent *S. aureus* ATCC12600^{GFP} (10^9 bacteria ml^{-1} , 200 μl) underneath the AIW glass (but not onto the glass) to grow a biofilm.

In vivo self-targeting of micelles to an infectious staphylococcal biofilm grown underneath an AIW in mice

After 48 hours of biofilm growth underneath the window, mice were anaesthetized and Nile red-loaded ZW-MSPM or SSPM suspensions (PBS at pH 7.4; 500 $\mu\text{g ml}^{-1}$) were injected in the tail (200 μl), immediately after which intravital images were taken as a function of time up to 30 min to monitor biofilm targeting by ZW-MSPMs. In vivo self-targeting of micelles was monitored in three mice.

In vivo eradication of a staphylococcal infection underneath an AIW in mice by micelles in combination with ciprofloxacin

To monitor the biofilm eradication in vivo, mice were first injected in the tail with 200 μl of PBS (pH 7.4) or a suspension of SSPMs and ZW-MSPMs (PBS at pH 7.4; 200 $\mu\text{g ml}^{-1}$), immediately followed

by 200 μl of ciprofloxacin in PBS (1 mg ml^{-1}). The consecutive injection scheme was repeated daily until the end of the experimental period, and intravital images were acquired each day after injection.

Intra-abdominal imaging in living mice

For intra-abdominal imaging, mice were anesthetized and placed on a custom-designed stage of a two-photon laser scanning confocal microscope (Olympus Corporation, Tokyo, Japan; FV1200 MPE), with the window frame fixed in a clamp to ensure proper focusing over time. After intra-abdominal imaging, images were analyzed using ImageJ software. Each three-dimensional (3D) image stack was processed using Fiji's 3D viewer plugin (60).

Tissue analyses

The mice were sacrificed 5 days after initiating treatment. After sacrifice, the AIW was removed and the wound tissues were collected and placed in sterile PBS. Tissue samples of each mouse were complemented with scrapings from the AIW that may have contained adhering biofilm, homogenized, serially diluted, and plated on TSB agar plates, and after 18 hours of incubation at 37°C, the CFUs were counted. Blood samples were collected from eyes for routine analyses, while major organs including the heart, lung, liver, spleen, and kidney were removed, followed by hematoxylin and eosin staining and microscopic examination.

Statistical analysis

All data are expressed as means \pm SD. Differences between groups were examined for statistical significance using a two-tailed Student's *t* test.

SUPPLEMENTARY MATERIALS

Supplementary material for this article is available at <http://advances.sciencemag.org/cgi/content/full/6/33/eabb1112/DC1>

REFERENCES AND NOTES

1. Y. Liu, L. Shi, L. Su, H. C. van der Mei, P. C. Jutte, Y. Ren, H. J. Busscher, Nanotechnology-based antimicrobials and delivery systems for biofilm-infection control. *Chem. Soc. Rev.* **48**, 428–446 (2019).
2. D. Davies, Understanding biofilm resistance to antibacterial agents. *Nat. Rev. Drug Discov.* **2**, 114–122 (2003).
3. J. O'Neill, Antimicrobial resistance: Tackling a crisis for the health and wealth of nations. Review on antimicrobial resistance (Creative Commons Attribution 4.0 International Public Licence, 2014).
4. A. J. Huh, Y. J. Kwon, "Nanoantibiotics": A new paradigm for treating infectious diseases using nanomaterials in the antibiotics resistant era. *J. Control. Release* **156**, 128–145 (2011).
5. S. J. Howard, S. Hopwood, S. C. Davies, Antimicrobial resistance: A global challenge. *Sci. Transl. Med.* **6**, 236ed210 (2014).
6. H. Koo, R. N. Allan, R. P. Howlin, P. Stoodley, L. Hall-Stoodley, Targeting microbial biofilms: Current and prospective therapeutic strategies. *Nat. Rev. Microbiol.* **15**, 740–755 (2017).
7. X. Ding, A. Wang, W. Tong, F.-J. Xu, Biodegradable antibacterial polymeric nanosystems: A new hope to cope with multidrug-resistant bacteria. *Small* **15**, e1900999 (2019).
8. A. Vermote, G. Brackman, M. D. P. Risseuw, B. Vanhoutte, P. Cos, K. Van Hecke, K. Breyne, E. Meyer, T. Coenye, S. Van Calenberg, Hamamelitannin analogues that modulate quorum sensing as potentiators of antibiotics against *Staphylococcus aureus*. *Angew. Chem. Int. Ed. Engl.* **55**, 6551–6555 (2016).
9. H.-C. Flemming, J. Wingender, U. Szewzyk, P. Steinberg, S. A. Rice, S. Kjelleberg, Biofilms: An emergent form of bacterial life. *Nat. Rev. Microbiol.* **14**, 563–575 (2016).
10. V. Berk, J. C. N. Fong, G. T. Dempsey, O. N. Develioğlu, X. Zhuang, J. Liphardt, F. H. Yildiz, S. Chu, Molecular architecture and assembly principles of *Vibrio cholerae* biofilms. *Science* **337**, 236–239 (2012).
11. A. W. Smith, Biofilms and antibiotic therapy: Is there a role for combating bacterial resistance by the use of novel drug delivery systems? *Adv. Drug Deliv. Rev.* **57**, 1539–1550 (2005).

12. P. S. Stewart, J. W. Costerton, Antibiotic resistance of bacteria in biofilms. *Lancet* **358**, 135–138 (2001).
13. J. N. Anderl, M. J. Franklin, P. S. Stewart, Role of antibiotic penetration limitation in *Klebsiella pneumoniae* biofilm resistance to ampicillin and ciprofloxacin. *Antimicrob. Agents Chemother.* **44**, 1818–1824 (2000).
14. J. L. del Pozo, R. Patel, The challenge of treating biofilm-associated bacterial infection. *Clin. Pharmacol. Ther.* **82**, 204–209 (2007).
15. H.-C. Flemming, J. Wingender, The biofilm matrix. *Nat. Rev. Microbiol.* **8**, 623–633 (2010).
16. J. B. Kaplan, Biofilm dispersal: Mechanisms, clinical implications, and potential therapeutic uses. *J. Dent. Res.* **89**, 205–218 (2010).
17. S. A. West, A. S. Griffin, A. Gardner, S. P. Diggle, Social evolution theory for microorganisms. *Nat. Rev. Microbiol.* **4**, 597–607 (2006).
18. D. McDougald, S. A. Rice, N. Barraud, P. D. Steinberg, S. Kjelleberg, Should we stay or should we go: Mechanisms and ecological consequences for biofilm dispersal. *Nat. Rev. Microbiol.* **10**, 39–50 (2011).
19. S. A. Rice, C. H. Tan, P. J. Mikkelsen, V. Kung, J. Woo, M. Tay, A. Hauser, D. McDougald, J. S. Webb, S. Kjelleberg, The biofilm life cycle and virulence of *Pseudomonas aeruginosa* are dependent on a filamentous prophage. *ISME J.* **3**, 271–282 (2009).
20. M. Okshevsky, V. R. Regina, R. L. Meyer, Extracellular DNA as a target for biofilm control. *Curr. Opin. Biotechnol.* **33**, 73–80 (2015).
21. H. T. T. Duong, K. Jung, S. K. Kutty, S. Agustina, N. N. M. Adnan, J. S. Basuki, N. Kumar, T. P. Davis, N. Barraud, C. Boyer, Nanoparticle (star polymer) delivery of nitric oxide effectively negates *Pseudomonas aeruginosa* biofilm formation. *Biomacromolecules* **15**, 2583–2589 (2014).
22. N. Barraud, B. G. Kardak, N. R. Yepuri, R. P. Howlin, J. S. Webb, S. N. Faust, S. Kjelleberg, S. A. Rice, M. J. Kelso, Cephalosporin-3'-diazemiumdiolates: Targeted NO-donor prodrugs for dispersing bacterial biofilms. *Angew. Chem. Int. Ed.* **51**, 9057–9060 (2012).
23. T.-K. Nguyen, R. Selvanayagam, K. K. K. Ho, R. Chen, S. K. Kutty, S. A. Rice, N. Kumar, N. Barraud, H. T. T. Duong, C. Boyer, Co-delivery of nitric oxide and antibiotic using polymeric nanoparticles. *Chem. Sci.* **7**, 1016–1027 (2016).
24. N. Barraud, M. V. Storey, Z. P. Moore, J. S. Webb, S. A. Rice, S. Kjelleberg, Nitric oxide-mediated dispersal in single- and multi-species biofilms of clinically and industrially relevant microorganisms. *J. Microbiol. Biotechnol.* **2**, 370–378 (2009).
25. H.-C. Flemming, T. R. Neu, D. J. Wozniak, The EPS matrix: The "house of biofilm cells". *J. Bacteriol.* **189**, 7945–7947 (2007).
26. H.-C. Flemming, EPS—Then and now. *Microorganisms* **4**, 41 (2016).
27. C. B. Whitchurch, T. Tolker-Nielsen, P. C. Ragas, J. S. Mattick, Extracellular DNA required for bacterial biofilm formation. *Science* **295**, 1487 (2002).
28. J. J. T. M. Swartjes, T. Das, S. Sharifi, G. Subbiahdoss, P. K. Sharma, B. P. Krom, H. J. Busscher, H. C. van der Mei, A functional DNase I coating to prevent adhesion of bacteria and the formation of biofilm. *Adv. Funct. Mater.* **23**, 2843–2849 (2013).
29. E. A. Izano, M. A. Amarante, W. B. Kher, J. B. Kaplan, Differential roles of poly-N-acetylglucosamine surface polysaccharide and extracellular DNA in *Staphylococcus aureus* and *Staphylococcus epidermidis* biofilms. *Appl. Environ. Microbiol.* **74**, 470–476 (2008).
30. G. V. Tetz, N. K. Artemenko, V. V. Tetz, Effect of DNase and antibiotics on biofilm characteristics. *Antimicrob. Agents Chemother.* **53**, 1204–1209 (2009).
31. J. B. Kaplan, Therapeutic potential of biofilm-dispersing enzymes. *Int. J. Artif. Organs* **32**, 545–554 (2009).
32. J. B. Kaplan, C. Ragunath, N. Ramasubbu, D. H. Fine, Detachment of *Actinobacillus actinomycetemcomitans* biofilm cells by an endogenous β -hexosaminidase activity. *J. Bacteriol.* **185**, 4693–4698 (2003).
33. B. R. Boles, M. Thoendel, P. K. Singh, Rhamnolipids mediate detachment of *Pseudomonas aeruginosa* from biofilms. *Mol. Microbiol.* **57**, 1210–1223 (2005).
34. M. E. Davey, N. C. Caiazza, G. A. O'Toole, Rhamnolipid surfactant production affects biofilm architecture in *Pseudomonas aeruginosa* PAO1. *J. Bacteriol.* **185**, 1027–1036 (2003).
35. Y. Irie, G. A. O'Toole, M. H. Yuk, *Pseudomonas aeruginosa* rhamnolipids disperse *Bordetella bronchiseptica* biofilms. *FEMS Microbiol. Lett.* **250**, 237–243 (2005).
36. K. Forier, K. Raemdonck, S. C. De Smedt, J. Demeester, T. Coenye, K. Braeckmans, Lipid and polymer nanoparticles for drug delivery to bacterial biofilms. *J. Control. Release* **190**, 607–623 (2014).
37. M. L. Immordino, F. Dosio, L. Cattel, Stealth liposomes: Review of the basic science, rationale, and clinical applications, existing and potential. *Int. J. Nanomedicine* **1**, 297–315 (2006).
38. D. Borisova, E. Haladjova, M. Kyulavska, P. Petrov, S. Pispas, S. Stoitsova, T. Paunova-Krasteva, Application of cationic polymer micelles for the dispersal of bacterial biofilms. *Eng. Life Sci.* **18**, 943–948 (2018).
39. A. K. Lam, C. L. Wouters, E. L. Moen, J. Pusavat, C. V. Rice, Antibiofilm synergy of β -lactams and branched polyethylenimine against methicillin-resistant *Staphylococcus epidermidis*. *Biomacromolecules* **20**, 3778–3785 (2019).
40. Y. Liu, H. J. Busscher, B. Zhao, Y. Li, Z. Zhang, H. C. van der Mei, Y. Ren, L. Shi, Surface-adaptive, antimicrobially loaded, micellar nanocarriers with enhanced penetration and killing efficiency in staphylococcal biofilms. *ACS Nano* **10**, 4779–4789 (2016).
41. Y. Liu, H. C. van der Mei, B. R. Zhao, Y. Zhai, T. J. Cheng, Y. F. Li, Z. K. Zhang, H. J. Busscher, Y. J. Ren, L. Q. Shi, Eradication of multidrug-resistant staphylococcal infections by light-activatable micellar nanocarriers in a murine model. *Adv. Funct. Mater.* **27**, 1701974 (2017).
42. L. Ritsma, E. J. Steller, S. I. Ellenbroek, O. Kranenburg, I. H. Borel Rinkes, J. van Rheenen, Surgical implantation of an abdominal imaging window for intravital microscopy. *Nat. Protoc.* **8**, 583–594 (2013).
43. H. Gao, T. Cheng, J. Liu, J. Liu, C. Yang, L. Chu, Y. Zhang, R. Ma, L. Shi, Self-regulated multifunctional collaboration of targeted nanocarriers for enhanced tumor therapy. *Biomacromolecules* **15**, 3634–3642 (2014).
44. N. Høiby, T. Bjarnsholt, C. Moser, G. L. Bassi, T. Coenye, G. Donelli, L. Hall-Stoodley, V. Høla, C. Imbert, K. Kirketerp-Møller, D. Lebeaux, A. Oliver, A. J. Ullmann, C. Williams, ESCMID guideline for the diagnosis and treatment of biofilm infections 2014. *Clin. Microbiol. Infect.* **21** (Suppl. 1), S1–S25 (2015).
45. A. Heydorn, A. T. Nielsen, M. Hentzer, C. Sternberg, M. Givskov, B. K. Ersboll, S. Molin, Quantification of biofilm structures by the novel computer program COMSTAT. *Microbiol.* **146** (Pt. 10), 2395–2407 (2000).
46. L. Wang, Y. Miao, M. Lu, Z. Shan, S. Lu, J. Hou, Q. Yang, X. Liang, T. Zhou, D. Curry, K. Oakes, X. Zhang, Chloride-accelerated Cu-Fenton chemistry for biofilm removal. *Chem. Commun.* **53**, 5862–5865 (2017).
47. L. Gao, K. M. Giglio, J. L. Nelson, H. Sondermann, A. J. Travis, Ferromagnetic nanoparticles with peroxidase-like activity enhance the cleavage of biological macromolecules for biofilm elimination. *Nanoscale* **6**, 2588–2593 (2014).
48. E. Tayeb-Figlelman, O. Tabachnikov, A. Moshe, O. Goldschmidt-Tran, M. R. Sawaya, N. Coquelle, J. P. Colletier, M. Landau, The cytotoxic *Staphylococcus aureus* PSM α 3 reveals a cross- α amyloid-like fibril. *Science* **355**, 831–833 (2017).
49. N. Paranjayy, V. Daggett, De novo designed α -sheet peptides inhibit functional amyloid formation of *Streptococcus mutans* biofilm. *J. Mol. Biol.* **430**, 3764–3773 (2018).
50. A. Bleem, R. Francisco, J. D. Bryers, V. Daggett, Designed alpha-sheet peptides suppress amyloid formation in *Staphylococcus aureus* biofilms. *NPJ Biofilms Microbiomes* **3**, 16 (2017).
51. L. Liu, K. Xu, H. Wang, P. K. Tan, W. Fan, S. S. Venkatraman, L. Li, Y.-Y. Yang, Self-assembled cationic peptide nanoparticles as an efficient antimicrobial agent. *Nat. Nanotechnol.* **4**, 457–463 (2009).
52. X. Jin, Y.-H. Xiong, X.-Y. Zhang, R. X. Wang, Y. G. Xing, S. Duan, D. F. Chen, W. Tian, F.-J. Xu, Self-adaptive antibacterial porous implants with sustainable responses for infected bone defect therapy. *Adv. Funct. Mater.* **29**, 1807915 (2019).
53. H. J. Busscher, W. Woudstra, T. G. van Kooten, P. Jutte, L. Shi, J. Liu, W. L. J. Hinrichs, H. W. Frijlink, R. Shi, J. Liu, J. Parvizi, S. Kates, V. M. Rotello, T. P. Schaer, D. Williams, D. W. Grainger, H. C. van der Mei, Accepting higher morbidity in exchange for sacrificing fewer animals in studies developing novel infection-control strategies. *Biomaterials* **232**, 119737 (2020).
54. J. Aguiar, P. Carpena, J. A. Molina-Bolívar, C. Carnero Ruiz, On the determination of the critical micelle concentration by the pyrene 1:3 ratio method. *J. Colloid Interface Sci.* **258**, 116–122 (2003).
55. J. Li, H. J. Busscher, H. C. van der Mei, W. Norde, B. P. Krom, J. Sjollem, Analysis of the contribution of sedimentation to bacterial mass transport in a parallel plate flow chamber: Part II: Use of fluorescence imaging. *Colloids Surf. B Biointerfaces* **87**, 427–432 (2011).
56. D. Hu, Y. Deng, F. Jia, Q. Jin, J. Ji, Surface charge switchable supramolecular nanocarriers for nitric oxide synergistic photodynamic eradication of biofilms. *ACS Nano* **14**, 347–359 (2020).
57. G. Qi, F. Hu, Kenry, L. Shi, M. Wu, B. Liu, An AIEgen-peptide conjugate as a phototheranostic agent for phagosome-entrapped bacteria. *Angew. Chem. Int. Ed.* **58**, 16229–16235 (2019).
58. P. V. Turner, T. Brabb, C. Pekow, M. A. Vasbinder, Administration of substances to laboratory animals: Routes of administration and factors to consider. *J. Am. Assoc. Lab. Anim. Sci.* **50**, 600–613 (2011).
59. P. Vachon, S. Faubert, D. Blais, A. Comtois, J. G. Bienvenu, A pathophysiological study of abdominal organs following intraperitoneal injections of chloral hydrate in rats: Comparison between two anaesthesia protocols. *Lab. Anim* **34**, 84–90 (2000).
60. B. Schmid, J. Schindelin, A. Cardona, M. Longair, M. Heisenberg, A high-level 3D visualization API for Java and ImageJ. *BMC Bioinformatics* **11**, 274 (2010).

Acknowledgments

Funding: This work was financially supported by the National Natural Science Foundation of China (nos. 21620102005, 51933006, and 81722026), the CAMS Innovation Fund for Medical Sciences (2016-I2M-3-022), and the Non-profit Central Research Institute Fund of Chinese Academy of Medical Sciences (2019-RC-HL-014). **Author contributions:** S.T., Y.L., F.H., J.L.,

Y.A., H.J.B., and L.Sh. designed experiments. S.T., L. Su, J.C., and G.Y. performed experiments. S.T. and H.J.B. wrote the manuscript. Y.R., H.J.B., H.C.v.d.M., and L.Sh. edited the manuscript. All the authors analyzed the data and contributed to the paper. **Competing interests:** H.J.B. is the director-owner of a consulting company, SASA BV. The authors declare that they have no potential competing interests with respect to authorship and/or publication of this article. **Data and materials availability:** All data needed to evaluate the conclusions in the paper are present in the paper and/or the Supplementary Materials. Additional data related to this paper may be requested from the authors.

Submitted 30 January 2020
Accepted 1 July 2020
Published 14 August 2020
10.1126/sciadv.abb1112

Citation: S. Tian, L. Su, Y. Liu, J. Cao, G. Yang, Y. Ren, F. Huang, J. Liu, Y. An, H. C. van der Mei, H. J. Busscher, L. Shi, Self-targeting, zwitterionic micellar dispersants enhance antibiotic killing of infectious biofilms—An intravital imaging study in mice. *Sci. Adv.* **6**, eabb1112 (2020).